

## THE FINAL-PARSEC PROBLEM IN NONSPHERICAL GALAXIES REVISITED

EUGENE VASILIEV<sup>1,2</sup>, FABIO ANTONINI<sup>3</sup>, AND DAVID MERRITT<sup>2</sup>

<sup>1</sup>Lebedev Physical Institute, Moscow, Russia

<sup>2</sup>School of Physics and Astronomy and Center for Computational Relativity and Gravitation,  
Rochester Institute of Technology, Rochester, NY 14623, USA and

<sup>3</sup>Canadian Institute for Theoretical Astrophysics, University of Toronto, Toronto, Ontario, Canada

*Draft version July 20, 2018*

### ABSTRACT

We consider the evolution of supermassive black hole binaries at the center of spherical, axisymmetric, and triaxial galaxies, using direct  $N$ -body integrations as well as analytic estimates. We find that the rates of binary hardening exhibit a significant  $N$ -dependence in all the models, at least for  $N$  in the investigated range of  $10^5 \leq N \leq 10^6$ . Binary hardening rates are also substantially lower than would be expected if the binary “loss cone” remained “full,” as it would be if the orbits supplying stars to the binary were being efficiently replenished. The difference in binary hardening rates between the spherical and nonspherical models is less than a factor of two even in the simulations with the largest  $N$ . By studying the orbital populations of our models, we conclude that the rate of supply of stars to the binary via draining of centrophilic orbits is indeed expected to be much lower than the full-loss-cone rate, consistent with our simulations. We argue that the binary’s evolution in the simulations is driven in roughly equal amounts by collisional and collisionless effects, even at the highest  $N$ -values currently accessible. While binary hardening rates would probably reach a limiting value for large  $N$ , our results suggest that we cannot approach that rate with currently available algorithms and computing hardware. The extrapolation of results from  $N$ -body simulations to real galaxies is therefore not straightforward, casting doubt on recent claims that triaxiality or axisymmetry alone are capable of solving the final-parsec problem in gas-free galaxies.

*Subject headings:* galaxies: elliptical and lenticular, cD – galaxies: evolution – galaxies: kinematics and dynamics – galaxies: nuclei

### 1. INTRODUCTION

According to large-scale simulations of the clustering of dark matter in the universe, the mean time between major mergers of dark halos varies between  $\sim 0.2$  Gyr at a redshift  $z = 10$  and  $\sim 10^{10}$  yr at  $z = 1$ , with a weak dependence on halo mass (Fakouri et al. 2010). Mergers between halo-sized objects are expected to bring the baryonic components together in a time comparable to the halo coalescence time (White & Rees 1978; Barnes 2001). By the same reasoning, if each merging galaxy contained a central supermassive black hole (SMBH), the two SMBHs would form a bound system in the merged galaxy – a binary SMBH – shortly after the merger was complete (Begelman et al. 1980; Roos 1981). This idea has received considerable attention because the ultimate coalescence of such a binary would generate an observable outburst of gravitational waves (GWs; Thorne & Braginskii 1976).

Begelman et al. (1980) pointed out a potential bottleneck in the evolution of binary SMBHs toward coalescence. The binary interacts with nearby stars, ejecting them with velocities comparable to the binary’s orbital velocity. This is the “gravitational slingshot” (Saslaw et al. 1974). But the process is self-limiting, and it is not a priori clear that the orbits will be repopulated in a time shorter than the age of the universe. This has been called the “final-parsec problem” (Milosavljevic & Merritt 2003a); the name derives from

the fact that the natural separation of a massive binary at the center of a galaxy is roughly a parsec.

Just as in the case of a *single* SMBH at the center of a galaxy, a binary SMBH can continue interacting with stars only if the relevant orbits – the “loss-cone” orbits – are repopulated. Repopulation of loss-cone orbits by gravitational encounters – i.e., collisional relaxation – is well understood in the context of single SMBHs in spherical galaxies (e.g., Lightman & Shapiro 1977; Cohn & Kulsrud 1978). Collisional effects are less well understood in the axisymmetric case (Magorrian & Tremaine 1999; Yu 2002; Vasiliev & Merritt 2013), and no such treatment exists yet for triaxial systems. Additional complications in the case of a binary SMBH include the likely anisotropy of the initial orbital distribution (just after formation of the hard binary), and the fact that the size of the loss region (= binary semimajor axis  $a$ ) changes with time.

Steady-state loss-cone theory (Merritt 2013, chapter 6) distinguishes between two regimes: the empty-loss-cone regime, in which the rate of repopulation of loss-cone orbits is slow enough that such orbits are fully depleted; and the full-loss-cone regime, which is reached when the encounter rate is so high that it is no longer a limiting factor. In the former case, the rate of orbital repopulation is inversely proportional to the relaxation time, which itself scales as  $\sim N/\ln N$  with the number of stars in the galactic nucleus (or particles in the  $N$ -body simulation), while in the latter case it saturates at a value that is essentially  $N$ -independent. The hardening rate of the binary,  $s \equiv d(1/a)/dt$ , is proportional to

the rate of repopulation of loss-cone orbits. Early  $N$ -body simulations of galaxies containing binary SMBHs adopted rather small  $N$ -values (Quinlan & Hernquist 1997; Milosavljević & Merritt 2001; Hemsendorf et al. 2002) and were essentially in the full-loss-cone regime, showing little or no dependence of  $s$  on  $N$ . More recent studies have verified that  $s$  drops with  $N$  for sufficiently high  $N$  (Makino & Funato 2004; Berczik et al. 2005; Merritt et al. 2007), as expected when approaching the empty-loss-cone regime. Approximate Fokker-Planck models of binary evolution in spherical galaxies (Milosavljević & Merritt 2003b; Merritt et al. 2007) also predict that the hardening rate of the binary should scale approximately as  $N^{-1}$  for large  $N$ .

Even in the absence of gravitational encounters, stars can continue to be supplied to the central binary if their orbital angular momenta are modified by torques from the nonspherical galaxy. This “collisionless” mode of loss-cone repopulation is essentially independent of the number of stars (in a galaxy of given size and mass) and can in principle provide stars to the central binary at high enough rates to ensure coalescence in a Hubble time (Merritt & Poon 2004; Holley-Bockelmann & Sigurdsson 2006). Some recent  $N$ -body simulations of galaxy mergers suggest in fact that the rates of binary evolution depend on  $N$  weakly, if at all, a result that the authors have attributed to the nonspherical shapes of the merged galaxies (Khan et al. 2011; Preto et al. 2011). However, other interpretations are possible for these intriguing results, due to the complex interplay between collisional and collisionless mechanisms. For instance, the size of the loss region, from which orbits can be driven into the loss cone via *collisionless* effects, is much larger in nonspherical systems than in spherical ones, hence, it can be more readily repopulated by *collisional* relaxation. Considerations like these suggest that it might be difficult to design an  $N$ -body simulation in which collisional effects would be truly negligible, as they are expected to be in many real galaxies.

In this paper we carry out direct  $N$ -body integrations of binary evolution in spherical, axisymmetric, and triaxial galaxies, constructed initially as equilibrium models. We do not simulate the galaxy merger process, and in this sense, our initial conditions can be considered less realistic than in some of the studies cited above. On the other hand, our method lends itself to a more rigorous comparison between binary evolution rates in galaxies with different geometries. We also carry out a much more detailed analysis of the orbital families in our models, and of the connection between orbital types and the binary evolution rates seen in the simulations.

## 2. NUMERICAL SIMULATIONS

### 2.1. Model construction

We considered three series of galaxy models having the same radial density profile but different degrees of asymmetry: spherical (S), oblate axisymmetric (A), and triaxial (T). The mass distributions were given in each case by a generalization of the Hernquist (1990) broken-

power-law model:

$$\rho(r) = \frac{M_{\text{total}}}{2\pi abc} \frac{1}{\tilde{r} (1 + \tilde{r})^3}, \quad (1)$$

$$\tilde{r}^2 \equiv \left(\frac{x}{a}\right)^2 + \left(\frac{y}{b}\right)^2 + \left(\frac{z}{c}\right)^2.$$

Axis ratios for the nonspherical models were  $a : b : c = 1 : 1 : 0.8$  (A) or  $1 : 0.9 : 0.8$  (T). We adopt units such that  $abc = M_{\text{total}} = 1$ . The potential of a central point mass,  $-GM_{\text{bin}}/r$ , representing the massive binary was added to the self-consistent potential of the stars; we consider a single value for  $M_{\text{bin}} = 10^{-2}$ , which is typical of previous studies. This is somewhat larger than the typical ratio  $\sim 10^{-3}$  of SMBH mass to galaxy mass (e.g. Marconi & Hunt 2003); however, since most stars that interact with the binary come from radii smaller than the scale radius of the model, restricting our consideration to the central parts of a galaxy is not likely to strongly affect the results. The distribution function for the spherical models was created using Eddington’s inversion formula (Merritt 2013, Equation (3.47)), which gives the unique, isotropic  $f(E)$  corresponding to a specified potential and density. The nonspherical {A, T} models were constructed by Schwarzschild (1979) orbit superposition method, using the publically available *SMILE* software (Vasiliev 2013) and  $10^5$  orbits. The nonspherical models are intrinsically anisotropic in velocity space, but we imposed “maximal isotropy” by requiring the velocity dispersion in the radial direction to equal one-half the sum of the velocity dispersions in the two transverse directions (no additional constraint was placed on the latter).

Monte Carlo realizations of each model were constructed for values of  $N$  in the range  $8 \times 10^3 \leq N \leq 10^6$ . We created several, independent realizations for each  $N$  (four for  $N \leq 125\text{K}$ , two for  $N = 250\text{K}$  and  $500\text{K}$ , one for  $N = 1000\text{K}$ ) because simulations with small  $N$  exhibit considerable scatter in the rate of evolution (e.g., Merritt et al. 2007). Unless otherwise specified, data plotted in the figures consist of values averaged over the multiple realizations.

We then replaced the single massive particle by two SMBH particles each of mass  $M_{\text{bin}}/2 = 5 \times 10^{-3}$  located symmetrically about the origin at  $x = \pm 0.1$  (as in Merritt et al. 2007). The initial separation was slightly larger than the radius of influence  $r_m$ , defined as the radius containing a stellar mass equal to  $2M_{\text{bin}}$ ; initially  $r_m \approx 0.15$  and  $r_m$  increases to about 0.2 as the central density drops. The initial velocities of the SMBH particles were set to 0.31 in model units, corresponding to a circular orbit in the  $x-y$  plane. In the course of the evolution, the eccentricity of the binary was found to remain low for  $N > 10^5$ , although it became somewhat larger for smaller  $N$ , with a large scatter between realizations; the average eccentricity was  $\approx 0.2(N/10^5)^{-1/2}$ .

We might also have placed just one SMBH particle at the origin and allowed the other to spiral in, or placed the two SMBHs symmetrically into an equilibrium model created without a central mass. We experimented with these and other configurations but found that the choice of initial placement affected only the initial stage of evolution, not the behavior at the hard binary stage.

We verified that the models so constructed were in

equilibrium by following their evolution for 20 time units (with a single central point mass) using the  $N$ -body code described below. No discernible evolution of the density profile or the model shapes was observed.

## 2.2. Parameters of the $N$ -body integrations

We used the direct  $N$ -body integrator  $\phi$ GRAPEch (Harfst et al. 2008) to follow the evolution of the massive binary. This code combines hardware-accelerated computation of pairwise interparticle forces (using the *Sapporo* library (Gaburov et al. 2009), which emulates the GRAPE interface utilizing GPU boards) with a high-accuracy chain regularization algorithm to follow the dynamical interactions of field stars with the two SMBH particles. The chain radius was set to  $4 \times 10^{-3}$  length units. In the present implementation, there could be only one chain which necessarily includes the first SMBH particle. Hence, in the early stages of evolution close approaches of field stars with the second SMBH particle were not regularized, which in principle might have led to the accumulation of errors; nevertheless, the relative error in total energy was typically  $\sim 10^{-4}$  for the accuracy parameter  $\eta = 0.01$  and even much smaller in the later stages of evolution ( $t \geq 30 - 40$  time units), when both SMBHs were included in the chain.

We used zero softening for interactions in the chain and set a very small softening length  $\epsilon = 10^{-6}$  outside the chain to prevent energy errors at the early integration stages. This is a much smaller softening length than the values typically used in other studies, and also much smaller than the distance of strong deflection for encounters between field stars; hence, we are guaranteed not to change the effective value of the Coulomb logarithm or the rate of relaxation. We checked this by repeating some simulations with  $\epsilon = 0$  at the late stages and verifying that there was no substantial difference in the binary hardening rate. Our experiments indicated that a larger value of softening length ( $\epsilon \geq 10^{-5}$ ) decreases the hardening rate and reduces the difference between simulations with different  $N$ , as well as between S, A, and T models.

## 2.3. Results

The models were evolved for 100 time units, with the final value of the binary semimajor axis,  $a$ , reaching  $a \lesssim (1 - 2.5) \times 10^{-3}$  length units depending on  $N$  and on model type (Figure 1). The elapsed time until formation of a “hard binary,”  $a \lesssim a_{\text{hard}}$ , was roughly  $t = 20$ ; we define  $a_{\text{hard}}$  in the standard way as

$$a_{\text{hard}} \equiv \frac{\mu}{M_{\text{bin}}} \frac{r_{\text{m}}}{4}, \quad \mu \equiv \frac{M_1 M_2}{M_1 + M_2} \quad (2)$$

(Merritt 2013, Equation (8.71)), with  $\mu$  the reduced mass of the binary. For our models,  $a_{\text{hard}} = r_{\text{m}}/16 \approx 10^{-2}$ .

Formation of the hard binary was accompanied by a substantial change in the density profile and in the distribution of particle energies in the models. Roughly speaking, the original  $\rho \sim r^{-1}$  cusp was replaced by a shallower,  $\rho \sim r^{-1/2}$  density profile inside  $r_{\text{m}}$ , corresponding to a mass deficit (Milosavljević et al. 2002) of order  $M_{\text{bin}}$ . The change in the energy distribution was more dramatic; almost no particles remained for energies  $|E| \gtrsim |\Phi_0| \approx 0.8$ , where  $\Phi_0$  is the depth of the potential

well due to the stars alone. In other words, there are almost no particles left that would be bound to the massive binary. In the course of subsequent evolution, the density profile and distribution function changed only modestly, the changes being spread over a much wider range of radii. Figure 2 shows that the axis ratios of the models at the hard binary stage, determined iteratively from the tensor of inertia of  $N$ -body snapshots (Katz 1991), were quite close to their values at  $t = 0$ . In other words, the binary has not destroyed the large-scale flattening or triaxiality, despite introducing some changes within the influence radius.

For  $t \gtrsim 30$ , the binary hardening rate  $s \equiv d(1/a)/dt$  was observed to be almost unchanging in each simulation. The hardening rate was computed as the slope of the inverse semimajor axis plotted as a function of time, calculated for several overlapping intervals of 20 time units on the interval  $30 \leq t \leq 100$  and averaged to get an estimate of scatter. We also averaged the results over the different realizations with the same  $N$ , adding the scatter to the error bars. Figure 3, top panel, shows that for low  $N$  ( $\lesssim 3 \times 10^4$ ) there is little difference between the three models and a weak dependence on  $N$ , consistent with earlier studies that also used small particle numbers (Quinlan & Hernquist 1997; Milosavljević & Merritt 2001; Chatterjee et al. 2003). For  $N \gtrsim 10^5$  the spherical model demonstrates a clear dependence of hardening rate on  $N$ , approximately as  $s \propto N^{-0.5}$ , again in agreement with earlier studies (Makino & Funato 2004; Berczik et al. 2005), and consistent with theoretical models of collisional loss-cone refilling (Merritt et al. 2007).

Hardening rates in the nonspherical models A and T are somewhat larger than in the spherical model, and quite close to each other, the difference appearing only for the  $N = 10^6$  model. But – contrary to our initial expectations, based on the galaxy merger studies cited in Section 1 – the hardening rates still exhibit a clear  $N$ -dependence at large  $N$ , suggesting a continued role for collisional orbital repopulation in these models.

## 3. ANALYSIS OF HARDENING RATES

### 3.1. Predictions from scattering experiments

To understand the binary evolution found in the simulations, we begin by considering the hardening rate due to the interaction between the binary and incoming stars in the  $N$ -body models. Following Hills (1983), we define the dimensionless coefficient  $C$  describing the energy exchange in one interaction between a “field” star of mass  $m_*$  and a massive binary:

$$C \equiv \frac{M_{\text{bin}}}{2m_*} \frac{\Delta E_{\text{bin}}}{E_{\text{bin}}}, \quad E_{\text{bin}} \equiv -\frac{GM_{\text{bin}}}{2a}. \quad (3)$$

The strength of an interaction can also be expressed in terms of the velocity at infinity,  $v$ , and impact parameter,  $b$ , of the incoming star. In the hard-binary limit,  $a \ll a_{\text{hard}}$ , the scattering outcome depends on a single dimensionless quantity

$$\chi \equiv \frac{L}{L_{\text{bin}}}, \quad L \equiv bv, \quad L_{\text{bin}} \equiv \sqrt{2GM_{\text{bin}}a}. \quad (4)$$

$\chi = 1$  corresponds to a distance of closest approach of the field star to the binary’s center of mass equal to  $a$ ,

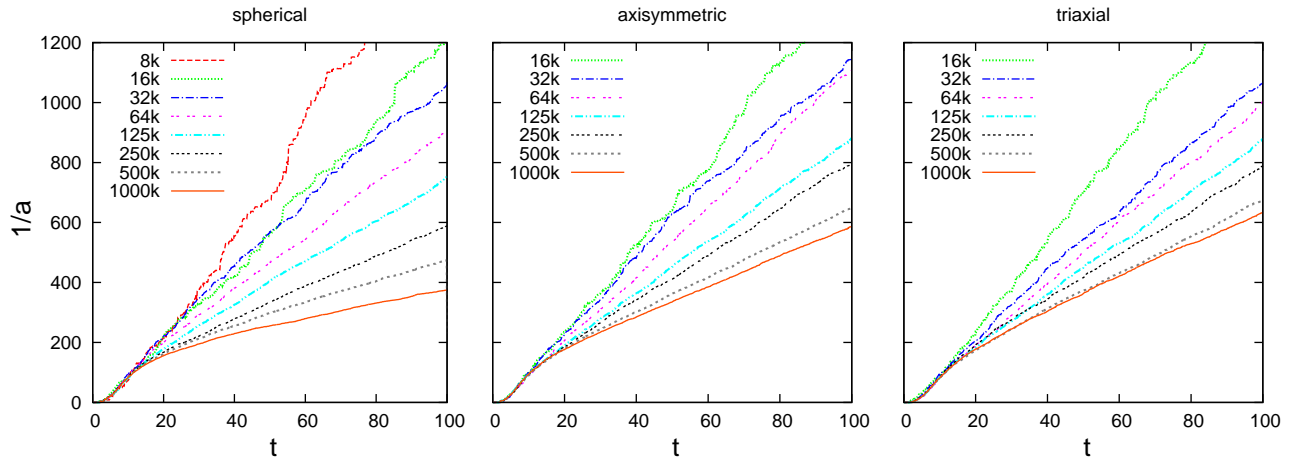


FIG. 1.— Evolution of binary hardness,  $1/a$ , as a function of time, for three series of models: spherical (left), axisymmetric (middle), and triaxial (right). Different curves are for models with  $N$  varying from  $8 \times 10^3$  to  $10^6$  (from top to bottom), averaged over several realizations with the same  $N$ , as discussed in the text.

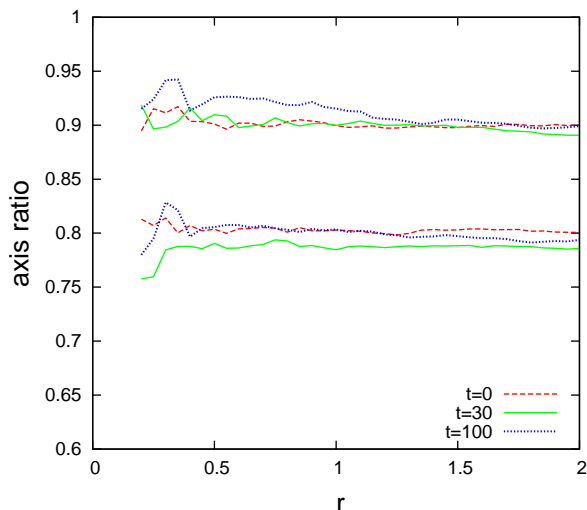


FIG. 2.— Axis ratios of the triaxial model with  $N = 10^6$  as a function of radius: initially (red), after formation of a hard binary ( $t = 30$ , green), and still further into the evolution ( $t = 100$ , blue). The model remains triaxial and close to its original shape.

if the binary were replaced by a single point mass. We adopt the dependence of  $C$  on  $\chi$  displayed in Figure 1 of Sesana et al. (2006), which we find to be reasonably well approximated (for a circular, equal-mass binary) by

$$C(\chi) \approx \begin{cases} 1.05 - 1.5\chi^2 + 21.67\chi^3 - 25\chi^4, & \chi < 0.6 \\ 1.95[1 + 7(\chi - 0.6)]e^{-7(\chi - 0.6)}, & \chi \geq 0.6 \end{cases} \quad (5)$$

We have ignored the dependence of the scattering cross section on the relative orientation of the binary's orbit and that of the incoming star. The change in binary hardness in one encounter is then given by

$$\Delta \left( \frac{1}{a} \right) = \frac{2m_\star}{M_{\text{bin}} a} C(\chi) \equiv \mathcal{H}(\chi). \quad (6)$$

Consider for the moment a model in which field stars are drawn from a homogeneous background with isotropically distributed velocities having a single magnitude  $v$ .

Then the hardening rate is

$$s \equiv \frac{d}{dt} \left( \frac{1}{a} \right) = \frac{\rho v}{m_\star} \int_0^\infty 2\pi b db \mathcal{H}(\chi) = \frac{G\rho}{v} H_0, \quad (7a)$$

$$H_0 \equiv \int_0^\infty 8\pi C(\chi) \chi d\chi. \quad (7b)$$

Integrating Equation (7b) using the expression (5) for  $C(\chi)$  yields  $H_0 \approx 18.5$ , almost the same as the value given by Quinlan (1996) in the hard-binary limit.

Next, we derive similar expressions for the hardening rate in the more realistic case where the distribution function of unbound stars has the form  $f(E, L)$ . We take into account that stars interact with the binary once per radial period  $T_{\text{rad}}$ , and that the number density of stars in  $\{E, L\}$  space is related to the phase-space mass density by  $dN = 8\pi^2 m_\star^{-1} T_{\text{rad}}(E, L) L f(E, L) dE dL$ . Then

$$\begin{aligned} s &= \int_{\Phi_0}^0 dE \int_0^{L_{\text{circ}}(E)} dL 8\pi^2 T_{\text{rad}} L \frac{f(E, L) 2m_\star C(L/L_{\text{bin}})}{m_\star M_{\text{bin}} a T_{\text{rad}}} \\ &= 4\pi G \int_{\Phi_0}^0 dE \int_0^{L_{\text{circ}}/L_{\text{bin}}} f(E, \chi L_{\text{bin}}) 8\pi \chi C(\chi) d\chi. \end{aligned} \quad (8)$$

Here  $\Phi_0$  is the lowest energy of an orbit unbound to the central object (equal to the depth of potential well produced by the stars), and  $L_{\text{circ}}(E)$  is the angular momentum of a circular orbit of energy  $E$ , which is much larger than  $L_{\text{bin}}$  in the limit of a hard binary. If the distribution function is isotropic, the hardening rate is given simply by (e.g., Merritt 2006, Equation 11)

$$s_{\text{iso}} = 4\pi G H_0 \int_{\Phi_0}^0 f(E) dE. \quad (9)$$

In the spherical case, this is the rate expected for the "full-loss-cone" regime, in which the initially isotropic distribution of orbits in angular momentum remains fixed (i.e. the loss cone is repopulated efficiently enough that we can neglect its depletion). In the nonspherical case, the rate would be roughly the same if we keep the orbit population fixed, even though any individual particle may precess into and out of the loss cone due to regular changes of angular momentum in addition to random

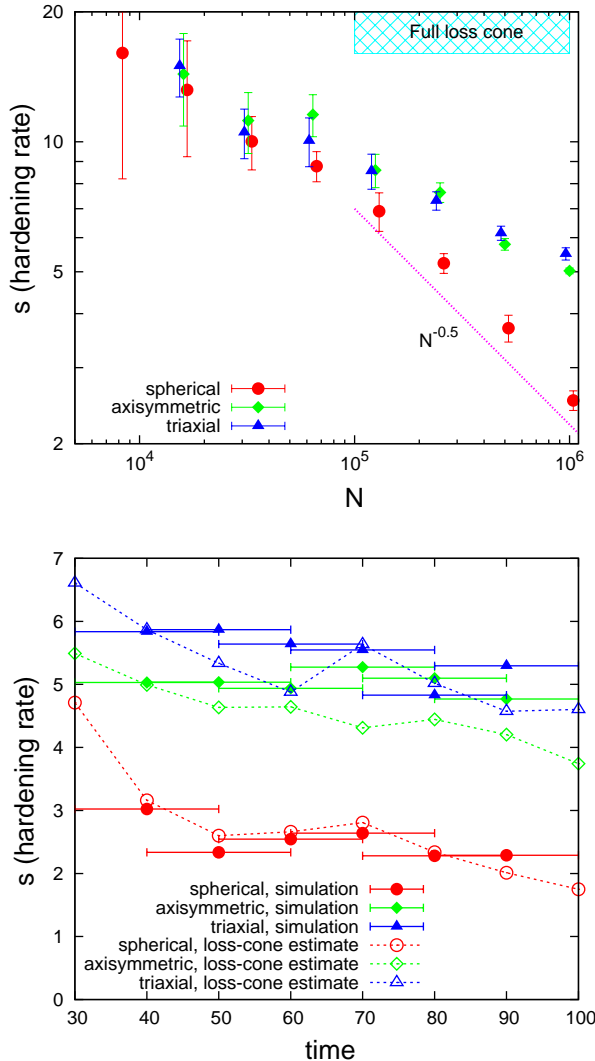


FIG. 3.— *Top panel:* hardening rates  $s \equiv (d/dt)(1/a)$  as a function of  $N$  for three series of models (red, spherical; green, axisymmetric; blue, triaxial), measured on the interval  $30 \leq t \leq 100$  (at the hard binary stage). Error bars reflect the variance seen in different realizations of the same model. The hardening rate for a full loss cone of the binary  $s = 18 \pm 2$  is marked by the hatched region on the plot.

*Bottom panel:* hardening rates as a function of time for  $N = 10^6$  models (colors are the same as in the top panel). Filled symbols with horizontal error bars show the estimate of the slope of  $1/a(t)$  on the corresponding interval of time; dashed lines with open symbols show the estimates from the loss-cone population (Equation 10) at corresponding moments of time. The two estimates agree quite well and have a rather moderate variation over time, with a weak tendency to decline.

perturbations. Alternatively, we could estimate the full-loss-cone hardening rate by taking the expression for the hardening rate in a homogeneous isothermal background,  $s = G\rho H/\sigma$ , with  $H \approx 15$  (Quinlan 1996; Sesana et al. 2006), and substituting the values of  $\sigma$  and  $\rho$  computed at the binary’s radius of influence (say), which yields a similar number. For our models during the late stages of evolution ( $t \gtrsim 30$ ), Equation (9) yields  $s \approx 18 \pm 2$ , almost independent of  $N$  and geometry. This value is consistent with the hardening rates observed in our lowest- $N$  simulations (Figure 3), but is several times *higher* than that

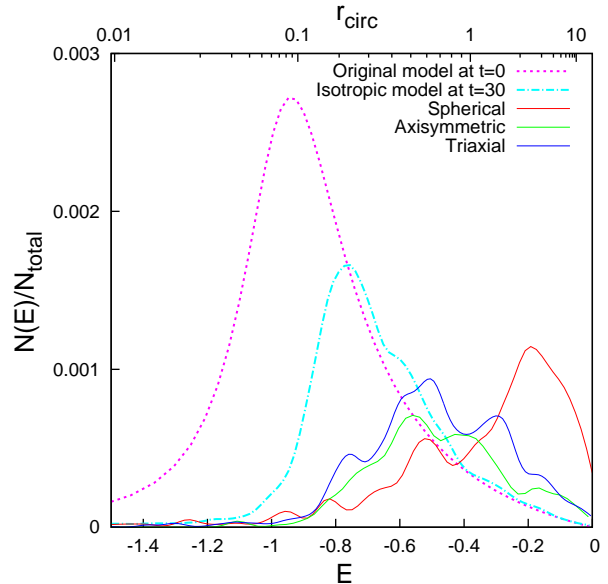


FIG. 4.— Population of stars in the loss cone (with angular momenta  $L < L_{\text{bin}} \equiv \sqrt{2GM_{\text{bin}}a}$ ) at  $t = 30$  ( $a = 1/250$ ) as a function of energy. Solid lines: the actual snapshots of spherical (red), axisymmetric (green), and triaxial (blue) models with  $10^6$  particles; cyan dot-dashed line: population in an isotropic model with the same density profile (i.e., full loss cone); dashed magenta line: same in the original model (before the formation of a hard binary).

of the simulations with  $N = 10^6$ , for all three geometries: additional evidence that even our triaxial models are far from being in the full-loss-cone regime.

Another way to justify the conclusion just reached is by calculating  $s$  directly from the  $N$ -body discrete distribution function, by summing the contributions to energy exchange (6) for each particle with angular momentum  $L_i$  during its orbital period  $T_{\text{rad},i}$ :

$$s_{N\text{-body}} = \sum_{i=1}^N \frac{2m_i}{M_{\text{bin}}a T_{\text{rad},i}} C(L_i/L_{\text{bin}}). \quad (10)$$

Computed in this way, the predicted hardening rates for all three series of models agree quite well with those measured in the simulations (Figure 3, bottom panel). We then artificially randomized the directions of the velocities of all the stars, leaving their magnitudes unchanged, thus creating an isotropic stellar system, which we integrated forward in time. (This was only done for a spherical system, since it would break the self-consistency of the nonspherical ones). The measured hardening rate was found to briefly jump to the full-loss-cone value for 1–2 time units before returning to the previous value.

The degree of loss-cone depletion can be quantified by plotting the actual population of particles on loss-cone orbits as a function of energy and comparing it with the isotropic case. Figure 4 shows that indeed the population of low angular momentum stars is much depleted compared with that of an isotropic model. For the S model, however, there is an *excess* of stars with low binding energies in the loss cone. These are the stars that have interacted once with the binary but that remained bound

by the galactic potential, making them candidates for the secondary slingshot process (Milosavljević & Merritt 2003b). Interestingly, those stars are absent in A and T models, presumably because angular momentum is not conserved and they precess away from the loss cone.

### 3.2. Theoretical estimates

The analysis presented above showed that there is only a moderate difference in the degree of loss-cone depletion between the S, A and T models. The goal of this section is to explain that result, and to show that for the present simulations, we would not expect to be able to reliably distinguish between collisional and collisionless loss-cone refilling processes.

For this purpose, we develop a simplified model of collisionless draining of the “loss region,” defined as the region of phase space from which orbits of stars in a nonspherical potential are able to reach low enough angular momenta that they can interact with the binary. (By contrast, the “loss cone” is the subset of trajectories in the loss region that are destined to pass near the binary in a single radial period or less.) This treatment is similar to the orbital draining models considered by Yu (2002), Merritt & Poon (2004), Merritt & Wang (2005), and Sesana et al. (2007) for a binary black hole, or by Vasiliev & Merritt (2013) for a single black hole in an axisymmetric galaxy, but is more realistic in that we: (1) use the actual orbit population of the  $N$ -body simulations; (2) take into account the movement of orbits into and out of the loss cone due to torquing by the mean-field potential; and (3) adopt a time-dependent size of the loss region around the central object.

First, we take a snapshot from the actual simulation at  $t = 30$ , when the initial stage of rapid evolution of the density profile has finished and a constant hardening rate of the binary has set in. We study the orbital population of the model by extracting a sample of  $10^5$  particles from the snapshot and evolving them in a fixed background potential corresponding to the same snapshot (plus one central point of mass  $M_{\text{bin}}$ ), but represented as a combination of smooth functions of radius times spherical harmonic functions of the angles  $(\theta, \phi)$  (up to  $l_{\text{max}} = 6$  in angular harmonics, keeping only triaxial or axisymmetric terms as appropriate; see Vasiliev (2013) for details). We then follow each orbit for  $200 T_{\text{rad}}(E)$ , which is long enough to build a meaningful distribution of values of the angular momentum at times of pericenter passage (see the Appendix for details). For a given orbit  $i$ , the probability of having  $L^2$  at pericenter below a certain value  $X$  is found to be well described by a linear function with slope  $\mathcal{S}_i^{-1}$ :

$$\mathcal{P}(L^2 < X) \approx \frac{X - L_{\text{min},i}^2}{\mathcal{S}_i}. \quad (11)$$

A zero value of  $L_{\text{min},i}$  indicates a truly centrophilic orbit, which can only exist in a triaxial potential; however, all orbits with  $L_{\text{min},i} \lesssim L_{\text{bin}}$  are “useful” for loss-cone repopulation. The combined mass of these orbits is 6% (1.5%) of the entire model for the T (A) case, i.e., substantially higher than the mass of the binary. We assume that values of  $L^2$  at subsequent pericenter passages are uncorrelated, which is reasonable given that most orbits of interest appear to be chaotic.

Next, we consider a time-dependent model for binary evolution that includes a depletion of orbits in the loss region. At each time step, we compute the instantaneous hardening rate according to Equation (10), with  $C(L_i/L_{\text{bin}})$  for each particle being averaged over all possible values of angular momentum at pericenter, weighted with the probability distribution (11):

$$s(t) \equiv \frac{d}{dt} \left( \frac{1}{a} \right) = \sum_{i=1}^N \frac{2m_i(t)}{M_{\text{bin}} a(t) T_{\text{rad},i}} \int_0^1 d\mathcal{P} C(\chi(\mathcal{P})) = \sum_{i=1}^N \frac{G m_i(t)}{\pi \mathcal{S}_i T_{\text{rad},i}} H_i(t), \quad (12a)$$

$$H_i \equiv \int_{\chi_{\text{min}}}^{\infty} 8\pi C(\chi) \chi d\chi, \quad \chi_{\text{min}} \equiv \frac{L_{\text{min},i}}{L_{\text{bin}}(t)} \quad (12b)$$

The quantity  $H_i$  equals the constant  $H_0$  (7b) for a centrophilic orbit ( $\chi_{\text{min}} = 0$ ), and tends to zero for orbits with  $L_{\text{min},i} \gtrsim 2L_{\text{bin}}$ .

Next we need to account for the decrease in the mass  $m_i$  associated with each orbit, since a star once scattered is assumed not to interact again with the binary. To account for this, we relate the evolution of  $a$  to the mass ejection rate, as described by a dimensionless coefficient

$$J \equiv \frac{a}{M_{\text{bin}}} \frac{dM_{\text{ej}}}{da} \quad (13)$$

(Quinlan 1996), and write

$$\frac{dM_{\text{ej}}}{dt} = - \sum_{i=1}^N \frac{dm_i}{dt} = J M_{\text{bin}} a s. \quad (14)$$

Identifying each term in this sum with the corresponding term in Equation (12) allows us to write the equation for the time evolution of the  $m_i$ :

$$\frac{dm_i}{dt} = -m_i \frac{G M_{\text{bin}} a(t) J H_i(t)}{\pi \mathcal{S}_i T_{\text{rad},i}} \quad (15)$$

This simplified treatment does not account for the variance in the outcome of scattering events with a given impact parameter, but is sufficient for the purposes of our estimate. The value of  $J$  is taken from Sesana et al. (2006); it has little dependence on  $a$  and lies in the range 0.5–1 and we took the former value, which was also found in the  $N$ -body simulations of Milosavljević & Merritt (2001). A higher value of  $J$  would decrease the late-time hardening rate, as the orbits would be depleted faster. Equations (12) and (15), together with the initial conditions  $a(0) = a_{\text{init}}$ ,  $m_i(0) = 1/N$  and the coefficients  $L_{\text{min},i}$ ,  $\mathcal{S}_i$ ,  $T_{\text{rad},i}$  derived from the orbit analysis, describe the time-dependent evolution of binary hardness in the presence of orbital draining due to non-conservation of angular momentum in a nonspherical background potential.

Figure 5 shows the predicted evolution of  $1/a$  in models T and A starting at  $t = 30$  and  $1/a = 250$ , compared with the actual evolution of  $1/a$  in the simulations with  $N = 10^6$ . We also show, for the spherical model, the evolution rate expected for the full-loss-cone case and for the actual population of loss-cone orbits. Two results are apparent: (1) binary hardening rates predicted

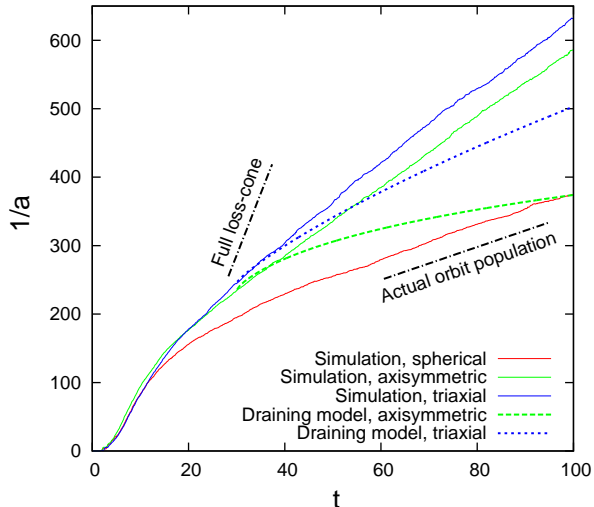


FIG. 5.— Evolution of binary hardness as a function of time. Solid lines: actual simulations with  $N = 10^6$ , from top to bottom: T, A and S models; dotted lines: predictions from collisionless draining models, obtained by integrating Equations (12) and (15) forward in time, starting at  $t = 30$  with  $1/a \simeq 250$ . Upper curve is for T model, lower is for A model; both are substantially lower than the actual hardening rates due to combined effects of draining and relaxation, and comparable to the hardening rate of the S model, which is due to relaxation only. Dot-dashed lines show the hardening rate expected in the full-loss-cone regime (Equation 9) and the one computed from the actual orbit population (Equation 10) for the spherical model.

by our (collisionless) machinery in the A and T models fall below the actual rates, but only by modest factors. In other words, collisional replenishment of the orbits is still contributing to the evolution of the binary in these models. (2) The hardening rates in the A and T models – both predicted and actual – fall substantially below the full-loss-cone rate. In other words, replenishment of orbits by torquing due to the nonspherical potential is not efficient enough to keep the loss-cone orbits fully occupied.

Figure 5 suggests that – even for this large number of particles – we cannot reliably discern the relative contribution of collisional and collisionless processes to the hardening rate. A consequence of this result is that it is difficult to extrapolate our results to the much higher  $N$  values relevant to real galaxies.

At the same time, our simplified model suggests that orbital draining can sustain a hardening rate that is several times below that of a full loss cone for a fairly long time in the triaxial case, as the total mass of stars on centrophilic orbits is a few times larger than  $M_{\text{bin}}$ . The situation is less clear for the axisymmetric models: on the one hand, there are no “genuinely centrophilic” orbits in this case; on the other hand, the reservoir of orbits that have low enough  $L_{\text{min}}$  to be able to interact with the binary is still much larger than the volume of the loss cone in the spherical case. The simplified calculation above predicts that the draining rate of this loss region is merely a factor of two lower than in the triaxial case, but that it may depend strongly on time.

### 3.3. Discussion

The rate of repopulation of loss-cone orbits is determined by a combination of collisional effects (due to gravitational encounters) and collisionless effects (due to torquing by a nonspherical potential). The former are well studied in the context of standard loss-cone theory. Approximate Fokker–Planck models for the binary evolution in the spherical geometry (Milosavljević & Merritt 2003b; Merritt et al. 2007) predict that the hardening rate should scale as  $s \propto N^{-1}$  for large  $N$  (when the system is fully in the empty-loss-cone regime), and the numerical simulations cited above show substantial  $N$ -dependence (although less steep than the prediction) for  $N \gtrsim 10^5$ .

The second mechanism of loss-cone repopulation, which can torque orbits from a much larger “loss region” into the loss cone, is collisionless and therefore does not depend on  $N$ . Still, in our  $N$ -body integrations, we have observed a substantial  $N$ -dependence in both the axisymmetric and triaxial cases. A simple model for draining of the loss region found that this mechanism could account for about one-half of the hardening rate seen in the simulations; the remainder would be attributed to  $N$ -dependent collisional effects. To reliably drive the latter below the expected rate of collisionless loss-cone repopulation would require a still much larger value of  $N$  – difficult to achieve with existing algorithms and hardware.

An additional complication arises from the complex interplay between collisional and collisionless factors: the size of the loss region, from which the orbits can be torqued into the loss cone due to collisionless effects, is much larger in nonspherical than in spherical systems, and hence can be more readily repopulated by *collisional* relaxation. For instance, Vasiliev & Merritt (2013) have shown that in a steady state, the rate of loss-cone repopulation for a single SMBH in an axisymmetric galaxy is a few times higher than in the corresponding spherical system. This makes it even more difficult to design an  $N$ -body simulation in which the collisional effects would be negligible, as they are expected to be in many real galaxies. While we certainly expect there to exist an effective lower limit, as a function of  $N$ , on the binary hardening rates in nonspherical galaxies, we are unable to make a precise statement concerning how low that rate might be. Our results suggest only that we cannot approach that rate with currently available algorithms and computing hardware.

The simple draining model considered in this paper does not account for a number of other processes that may be effective in the  $N$ -body simulations or in real galaxies: Brownian motion of the binary (Merritt 2001), the “secondary slingshot” (Milosavljević & Merritt 2003b), time-dependent perturbations to stellar orbits even far from the binary (Kandrup et al. 2003), changes in the stellar density profile due to continuous ejection of stars (Milosavljević & Merritt 2001), possible long-term changes in degree of triaxiality (Merritt & Quinlan 1998), among others. Clearly, a still more elaborate model, combining both collisionless and collisional processes, is desired to better understand the dynamics of binary SMBHs in galactic nuclei.

Even in the context of models like ours, binary harden-

ing rates will vary as a function of the degree of velocity anisotropy (i.e., the detailed orbital population), the radial density profile, the shape of the nuclear isodensity contours, etc. While exploring the full range of such variation is beyond the scope of this paper, we can make some general remarks. Observed galaxies exhibit a variety of nuclear density profiles, from nearly flat cores to nuclear star clusters having  $\rho \sim r^{-2}$ . At larger radii the density is almost always well fit by a Sersic or Einasto function. Varying the nuclear density profile would certainly affect the early hardening rate of a binary. As discussed above (Section 2.3), during the formation of a “hard” binary, the initial density cusp is converted into a shallower profile as stars bound to the binary are ejected. The same will be qualitatively true for any initial nuclear density profile, although one expects some dependence of the final profile on the initial profile (Milosavljević & Merritt 2001; Khan et al. 2012). A velocity distribution that is more or less anisotropic would also lead to higher or lower binary hardening rates, at least initially. With regard to changes in the shape of the model, the results obtained here suggest that in nonspherical geometries, even fairly radical shape changes (axisymmetric  $\rightarrow$  triaxial) have only modest consequences for binary hardening rates, and we expect the same to be true in nonspherical models with axis ratios different from those considered here.

Our results present an interesting contrast to those of other recent studies based on similar techniques. Khan et al. (2013) integrated spherical and axisymmetric models created initially in equilibrium, with density profiles and black hole masses essentially the same as in our models. While their binary hardening rate for a spherical model with  $N = 10^6$  is comparable to ours, their flattened models have a much higher hardening rate than ours, even exceeding our estimate for the full-loss-cone case (9). We also observed much less difference between the spherical and nonspherical models up to  $N = 10^6$ . The reasons for these differences are unknown to us; however, at face value, our results call into question the robustness of the conclusion reached by those authors that the final-parsec problem is “solved” in axisymmetric galaxies.

On the other hand, triaxial models formed by a bar instability in a rotating galaxy (Berczik et al. 2006), or by mergers of two galaxies (Khan et al. 2011; Preto et al. 2011), have shown essentially no dependence of the hardening rate on  $N$ . We speculate that this difference with our results might be due to the rotation of those models, to non-stationary clumpy structures in the case of the merger remnants, or to some other factor. More detailed study of the orbit populations could shed light on this mystery.

Merritt & Poon (2004) (MP04) analyzed the orbital populations in self-consistent, triaxial models of nuclei containing central SMBHs. In the context of scale-free models with a steep,  $\rho \sim r^{-2}$  density profile, they argued that collisionless feeding rates might be high enough to ensure coalescence of massive binaries in less than 10 Gyr, even in galaxies where the fraction of centrophilic orbits was small. The models of MP04 were both extreme (a steep density profile, maximal triaxiality) and idealized (scale-free, fixed potential). We attempted to verify their conclusions by creating a non-scale-free model

with similar central properties (a steep density cusp and strong triaxiality) and an SMBH mass of  $10^{-2}M_{\text{gal}}$ ; in this model the region extending to a few influence radii was still well inside the break radius. This model had  $\sim 15\%$  of its mass on chaotic/centrophilic orbits, somewhat more than in the models presented above. The time-dependent draining rate was then computed as described above, assuming an initial binary separation of  $0.5a_{\text{hard}}$ . Our results for  $a(t)$  were not precisely the same as those in MP04; in particular, the hardening rate was found to drop more rapidly with time,  $(a_{\text{hard}}/a) \sim t^{0.65}$ . But the value of  $(a/a_{\text{hard}})^{-1}$  after a time corresponding to several Gyr was  $\sim 10^3$ , i.e., more than enough to ensure GW coalescence on Gyr timescales.

This comparison highlights an important point: even a modest rate of binary evolution (due to stellar-dynamical interactions) can result in a separation small enough for GW emission to induce coalescence in less than a Hubble time. The time for a circular binary’s orbit to evolve, from  $a = a_0$  to  $a = 0$ , due to GW emission is

$$t_{\text{GW}} \equiv t(a=0) - t(a=a_0) = \frac{5}{256} \frac{c^5 a_0^4}{G^3 M_1 M_2 M_{\text{bin}}} \quad (16)$$

$$\approx 5.7 \times 10^6 \frac{(1+q)^2}{q} \left( \frac{a_0}{10^{-2} \text{ pc}} \right)^4 \left( \frac{M_{\text{bin}}}{10^8 M_{\odot}} \right)^{-3} \text{ yr}$$

with  $q \equiv M_2/M_1 \leq 1$  (Merritt 2013, Equation (4.241)). This time is less than 10 Gyr if

$$\left( \frac{a_0}{a_{\text{hard}}} \right)^4 \lesssim (1.3 \times 10^{14} \text{ yr}) \frac{(1+q)^6 G^3 M_{\text{bin}}^3}{q^3 c^5 r_m^4} \quad (17)$$

i.e. if

$$\frac{a_0}{a_{\text{hard}}} \lesssim 0.03 \frac{(1+q)^{3/2}}{q^{3/4}} \left( \frac{M_{\text{bin}}}{10^8 M_{\odot}} \right)^{3/4} \left( \frac{r_m}{10 \text{ pc}} \right)^{-1} \quad (18)$$

or in the units of our  $N$ -body models ( $a_{\text{hard}} \approx 0.01$ ,  $q = 1$ )

$$a_0 \lesssim 10^{-3} \left( \frac{M_{\text{bin}}}{10^8 M_{\odot}} \right)^{3/4} \left( \frac{r_m}{10 \text{ pc}} \right)^{-1}. \quad (19)$$

Assuming that we have nearly reached the asymptotic (large- $N$ ) limit in our simulations, Figure 1 suggests that the binaries in many galaxies would indeed be able to reach coalescence in a Hubble time.

#### 4. CONCLUSIONS

We carried out direct  $N$ -body integrations of binary supermassive black holes in spherical, axisymmetric, and triaxial models of galaxies, constructed initially as equilibrium models. Our integrations with particle numbers up to  $N = 10^6$  demonstrated that in all three geometries considered, the binary hardening rate  $s \equiv d(1/a)/dt$  ( $a =$  binary semimajor axis) at late times does depend on  $N$  and is several times below the rate computed assuming a full loss cone. The difference in hardening rates between the three models was quite modest – within a factor of two even for the simulations with largest  $N$  – and only in the largest- $N$  case was there a noticeable difference in  $s$  between the axisymmetric and triaxial geometries.

To assist in understanding these results, we computed the expected hardening rates based on known results from three-body scattering experiments, together with



the distribution of particles in energy and angular momentum in the  $N$ -body models. These predictions were found to agree well with the hardening rates obtained in the actual simulations. We also estimated, using a simple model for collisionless draining of orbits in the “loss region” (the collection of orbits that are able to reach the binary’s interaction sphere), the contribution of nonspherical torques to the rate of loss-cone repopulation, and we found it to be below or comparable to the contribution from collisional effects, even for the highest-resolution simulation of our set.

Based on these results, we argued that in order to reach a regime that is characteristic of massive galaxies (in which collisional effects are believed to be negligible), substantially higher values of  $N$  might be needed in the simulations. Until this is done, it is premature to state that the final-parsec problem in gas-free galaxies is

“solved” by assuming nonspherical geometries.

This work was supported by the National Science Foundation under grant no. AST 1211602 and by the National Aeronautics and Space Administration under grant No. NNX13AG92G. Part of this work was done at the Alajar meeting<sup>1</sup> and in the Henri Poincaré institute in Paris. Computations were performed on the GPUs of the CITA Sunnyvale cluster, as well as the ARC supercomputer at the SciNET HPC Consortium. SciNet is funded by the Canada Foundation for Innovation under the auspices of Compute Canada, the Government of Ontario, Ontario Research Fund Research Excellence, and the University of Toronto. We thank John Dubinski for assistance with the cluster.

## REFERENCES

- Barnes, J. 2001, in ASP conf. series, 245, *Astrophysical Ages and Times Scales*, ed. T. von Hippel, C. Simpson, & N. Manset, (San Francisco, CA: ASP), 382
- Begelman, M. C., Blandford, R. D., & Rees, M. J. 1980, *Nature*, 287, 307
- Berczik, P., Merritt, D., & Spurzem, R. 2005, *ApJ*, 633, 680
- Berczik, P., Merritt, D., Spurzem, R., & Bischof, H. 2006, *ApJL*, 642, L21
- Chatterjee, P., Hernquist, L., & Loeb, A. 2003, *ApJ*, 592, 32
- Cohn, H., & Kulsrud, R. 1978, *ApJ*, 226, 1087
- Fakhouri, O., Ma, C.-P., & Boylan-Kolchin, M. 2010, *MNRAS*, 406, 2267
- Gaburov, E., Harfst, S., & Portegies Zwart, S. 2009, *NewA*, 14, 630
- Harfst, S., Gualandris, A., Merritt, D., & Mikkola, S. 2008, *MNRAS*, 389, 2
- Hemsendorf, M., Sigurdsson, S., & Spurzem, R. 2002, *ApJ*, 581, 1256
- Hernquist, L. 1990, *ApJ*, 356, 359
- Hills, J. G. 1983, *AJ*, 88, 1269
- Holley-Bockelmann, K., & Sigurdsson, S. 2006, arXiv:astro-ph/0601520
- Kandrup, H., Sideris, I., Terzić, B., & Bohn, C. 2003, *ApJ*, 597, 111
- Katz, N. 1991, *ApJ*, 368, 325
- Khan, F. M., Holley-Bockelmann, K., Berczik, P., & Just, A. 2013, *ApJ*, 773, 100
- Khan, F. M., Just, A., & Merritt, D. 2011, *ApJ*, 732, 89
- Khan, F. M., Preto, M., Berczik, P., et al. 2012, *ApJ*, 749, 147
- Lightman, A., & Shapiro, S. 1977, *ApJ*, 211, 244
- Magorrian, J., & Tremaine, S. 1999, *MNRAS*, 309, 447
- Makino, J., & Funato, Y. 2004, *ApJ*, 602, 93
- Marconi, A., & Hunt, L. K. 2003, *ApJL*, 589, 21
- Merritt, D. 2001, *ApJ*, 556, 245
- Merritt, D. 2006, *ApJ*, 648, 976
- Merritt, D., 2013, *Dynamics and Evolution of Galactic Nuclei* (Princeton, NJ: Princeton Univ. Press)
- Merritt, D., Mikkola, S., & Szell, A. 2007, *ApJ*, 671, 53
- Merritt, D., & Poon, M.-Y. 2004, *ApJ*, 606, 788
- Merritt, D., & Quinlan, G. D. 1998, *ApJ*, 498, 625
- Merritt, D., & Wang, J. 2005, *ApJL*, 621, L101
- Milosavljević, M., & Merritt, D. 2001, *ApJ*, 563, 34
- Milosavljević, M., & Merritt, D. 2003a, in *AIP Conf. Proc.*, 686, *The Astrophysics of Gravitational Wave Sources*, ed. J. Centrella and S. Barnes (Melville, NY: AIP), 201
- Milosavljević, M., & Merritt, D. 2003b, *ApJ*, 596, 860
- Milosavljević, M., Merritt, D., Rest, A., & van den Bosch, F. C. 2002, *MNRAS*, 331, L51
- Preto, M., Berentzen, I., Berczik, P., & Spurzem, R. 2011, *ApJL*, 732, L26
- Quinlan, G. 1996, *NewA*, 1, 35
- Quinlan, G., & Hernquist, L. 1997, *NewA*, 2, 533
- Roos, N. 1981, *A&A*, 104, 218
- Saslaw, W. C., Valtonen, M. J., & Aarseth, S. J. 1974, *ApJ*, 190, 253
- Schwarzschild, M. 1979, *ApJ*, 232, 236
- Sesana, A., Haardt, F., & Madau, P. 2006, *ApJ*, 651, 392
- Sesana, A., Haardt, F., & Madau, P. 2007, *ApJ*, 660, 546
- Thorne, K. S., & Braginskii, V. B. 1976, *ApJL*, 204, 1
- Vasiliev, E. 2013, *MNRAS*, 434, 3174
- Vasiliev, E., & Merritt, D. 2013, *ApJ*, 774, 87
- White, S. D. M., & Rees, M. 1978, *MNRAS*, 183, 341
- Yu, Q. 2002, *MNRAS*, 331, 935

## APPENDIX

The analysis of draining rates in Section 3.2 necessitated an estimate of the minimum angular momentum  $L_{\min}$  attained by a given orbit in the smooth potential. Of course, no orbit can reach zero angular momentum on any finite time interval (unless it is specially arranged to do so), but one can nevertheless estimate whether there is a positive lower limit on  $L_{\min}$ , or whether it is compatible with being zero, by the following procedure.

We record the values of the squared angular momentum at pericenter passages  $L_{\text{peri},k}^2$  ( $k = 1..N_{\text{peri}}$ ) and sort them in ascending order. As discussed in the text, it happens that the distribution usually follows a linear trend at low  $L^2$ . We therefore fit a linear regression with and without a constant term:

$$L_{\text{peri},k}^2 = L_{\min}^2 + s \frac{k}{N_{\text{peri}}} + \delta_k = s' \frac{k}{N_{\text{peri}}} + \delta'_k, \quad k = 1..N_{\text{fit}}, \quad N_{\text{fit}} = 0.1 N_{\text{peri}}. \quad (1)$$

Here,  $s$ ,  $L_{\min}^2$  and  $s'$  are the coefficients of two- and one-parameter fits, and  $\delta_k$  and  $\delta'_k$  are the corresponding residuals. We assign the intrinsic dispersion of the values  $L_{\text{peri},k}^2$  from the condition that  $\chi^2$  per degree of freedom is unity in

<sup>1</sup> <http://members.aei.mpg.de/amaro-seoane/ALM13>

the two-parameter fit:  $\sigma^2 \equiv \left( \sum_{k=1}^{N_{\text{fit}}} \delta_k^2 \right) / (N_{\text{fit}} - 2)$ . Next we compare the statistical significance of the fits to find out whether to prefer the one-parameter fit (describing a centrophilic orbit) over the more general two-parameter one. The difference  $\Delta\chi^2$  between the one-parameter and two-parameter fits is given by

$$\Delta\chi^2 = (N_{\text{fit}} - 2) \left( \frac{\sum_{k=1}^{N_{\text{fit}}} \delta_k'^2}{\sum_{k=1}^{N_{\text{fit}}} \delta_k^2} - 1 \right). \quad (2)$$

Of course, the residuals in the one-parameter fit are always greater than in the two-parameter fit, but if they are “not too much” greater then we accept the hypothesis that  $L_{\text{min}}^2 = 0$ . More quantitatively, we accept the one-parameter fit if it is less than  $3\sigma$  away from the two-parameter fit, i.e., if  $\Delta\chi^2 < \Delta\chi_{3\sigma}^2 \equiv 11.8$ , the latter value being the  $3\sigma$  deviation for a  $\chi^2$  distribution with two degrees of freedom. Usually if this hypothesis is rejected (i.e., the orbit is labeled centrophobic), it is at the level of significance of many hundreds or thousands of  $\sigma$ . Finally, we take the values of  $L_{\text{min}}^2$  and  $s$  (or  $s'$ ) from the adopted regression to estimate the probability of having a given value of  $L_{\text{peri}}^2$  (Equation 11).